# Solar Cells Operating under Thermal Stress

Rodolphe Vaillon, Stéphanie Parola, Chrysovalantou Lamnatou, Daniel Chemisana

Cell Reports
Physical Science

CellPress
OPEN ACCESS

Review

# Solar Cells Operating under Thermal Stress

Rodolphe Vaillon,[1,*] Stéphanie Parola,[1] Chrysovalantou Lamnatou,[2] and Daniel Chemisana[2]

## SUMMARY

**Operating a solar cell under thermal stress at temperatures >100°C and up to 500°C seems counterintuitive because conversion efficiency drops dramatically. Even so, there are cases in which solar cells are in high-illumination high-temperature conditions, for near-the-sun space missions and in various terrestrial hybrid systems involving solar-to-thermal energy conversion. This review analyzes the progress of solar cells tested in the laboratory under thermal stress. The fundamental physics governing the thermal sensitivity of solar cells and the main criteria determining the ability of semiconductor materials to survive high temperatures are recalled. Materials and architectures of a selection of the solar cells tested so far are examined. Deviation from the Shockley-Queisser limit at each temperature is used for a fair assessment of the performances. Our analysis reveals the strengths and weaknesses of the existing technologies and the gaps to be filled to develop new classes of solar cells capable of withstanding high temperatures.**

## INTRODUCTION

A priori, it is not advisable to operate solar cells at high temperature. The reason is simple: conversion efficiency drops with temperature.[1] In spite of this, there are cases in which solar cells are put under thermal stress (Figure 1). First, solar arrays used in near-the-sun space missions are subjected to multiple adverse conditions.[2] Closeness to the sun means high illumination, as in the case of concentrating photovoltaics (CPVs) on Earth. However, in space, one can only have recourse to thermal radiation for dissipating heat, and spacecraft may even be subjected to additional planetary infrared radiation, as is the case for the missions to Mercury.[3-5] As a result of a high-illumination high-temperature (HIHT) environment, solar arrays for near-the-sun space missions are designed for reaching equilibrium temperatures typically >130°C[6] and possibly much higher.[7] Second, with the aim of better harvesting solar radiation on Earth, hybrid systems couple solar cells with devices involving solar-to-thermal energy conversion.[8,9] Hybrid photovoltaic-thermal (PV-T) collectors combine PV cells with a solar-thermal converter in which thermal energy is harvested by a solar absorber exchanging heat with a moving fluid.[10] Even though most commercial PV-T collectors operate at fluid temperatures ranging from 40°C to 80°C,[11] an increasing number of designs extend this range up to 100°C–250°C.[12] Hybrid photovoltaic-thermoelectric (PV-TE) electricity generators combine a solar cell with a thermoelectric generator (TEG) to complement solar-to-thermal with solid-state thermal-to-electrical energy conversion.[12-14] Interestingly, certain simulations show an optimal paring at a temperature of 450 K (~177°C),[15] hence, putting the solar cell under thermal stress. Hybrid photovoltaic-thermal concentrated solar power (PV-CSP) systems generate electricity with solar cells and a solar-to-thermal energy converter combined to a heat engine.[8] Among 3 possible configurations, 1 is with the PV cells operating at very high temperature, around and $\geq$400°C.[16]

[1]IES, Univ Montpellier, CNRS, 34095 Montpellier, France

[2]Applied Physics Section of the Environmental Science Department, University of Lleida, 25003 Lleida, Spain

*Correspondence: rodolphe.vaillon@ies.univ-montp2.fr

https://doi.org/10.1016/j.xcrp.2020.100267

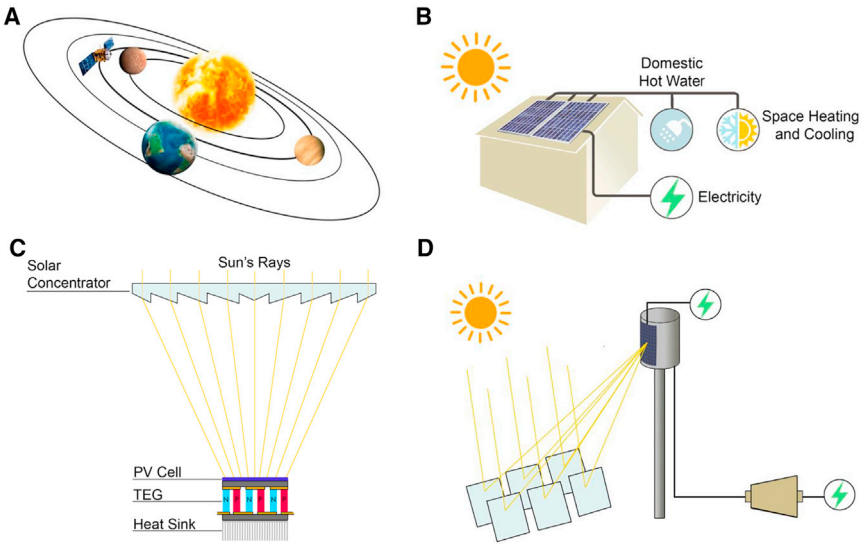


**Figure 1. Solar Cells Operating under Thermal Stress**

(A) Spatial solar cells in a high-illumination high-temperature (HIHT) environment.
(B–D) Terrestrial hybrid systems combining solar cells under thermal stress and devices involving solar-to-thermal energy conversion. (B) photovoltaic-thermal (PV-T), (C) photovoltaic-thermoelectric (PV-TE), and (D) photovoltaic-thermal concentrated solar power (PV-CSP) systems.

Even though the theoretical limiting efficiency of paired solar thermal-PV converters is large in ideal conditions,[17] in practice, solar cell conversion efficiency drops with temperature largely because of the non-fundamental losses.[18] A current challenge for conventional solar panels is to mitigate their thermal losses[19] in climate conditions in which their operating temperature does not exceed 70°C.[20] It follows that the challenge for fabricating solar cells supposed to optimally operate at temperatures from at least 100°C up to 550°C, either for near-the-sun space missions or in hybrid converters, is even greater.

In the present article, a state-of-the-art of solar cells operating under thermal stress, at temperatures >100°C, is established. In the following section, physics governing the sensitivity to temperature of solar cells is summarized, with an emphasis on the critical elements for pushing the limits to high-temperature levels. Then, materials and architectures selected thus far for testing solar cells at high temperature are described. The final section provides an overview of the performances of these solar cells in controlled laboratory conditions. Throughout the text, some key points for designing, fabricating, and testing these solar cells are highlighted.

## TEMPERATURE SENSITIVITY OF SOLAR CELLS IN A NUTSHELL

The base configuration for understanding the physics of the temperature sensitivity of solar cells is the so-called Shockley-Queisser (SQ) model. It defines an ideal situation with specific assumptions that sets an efficiency limit for solar cells.[21]. Having the meaning of this limit in mind, the fundamental losses can be calculated as a function of cell bandgap for a standard illumination[22] (Figure 2). An analysis of the dependence of these losses on cell temperature leads to determine how the ideal (SQ) limit is affected.[1,18]. In this frame, for a given bandgap, the ideal efficiency is a decreasing function of temperature, because radiative recombination rises exponentially with temperature. However, the bandgap of semiconductors varies with temperature (commonly through the so-called Varshni's equation[27]), meaning that

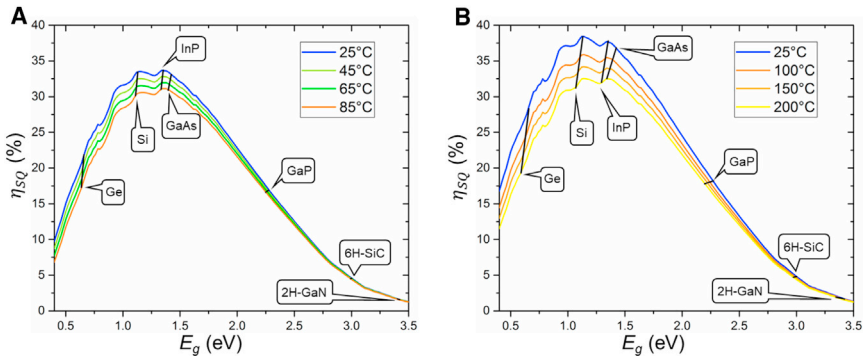


**Figure 2. Shockley-Queisser (SQ) Efficiency Limit as a Function of Bandgap Energy and Temperature**

(A) Under 1-sun illumination.

(B) Under 100-sun illumination.

The black lines depict the bandgap energy ($E_g$) variations with temperature of selected semiconductors, with data from Vaĭnshteĭn et al.[23] (Ge), Green[24] (Si), Galeckas et al.[25] (6H-SiC), and Vurgaftman et al.[26] (GaAs, InP, GaP, 2H-GaN).

the optimum bandgap choice at a moderate temperature may not remain so at higher temperatures. All the same, the SQ limit depends on illumination, hence on concentration (see, e.g., Zeitouny et al.[28]) and the spectrum.[29] As a result, a first-choice best bandgap based on the SQ limit requires us to consider both illumination and temperature.

This being stated, real solar cells do not operate at this ideal limit and certain losses must be added to the SQ fundamental ones.[30] In a nutshell, these losses come from non-ideal absorption, non-radiative recombination, and electrical resistance effects.[1,21,30] A recent state-of-the-art of solar cells shows how far from the ideal the current PV technologies are in the standard test conditions (STCs, i.e., under the AM1.5 spectrum illumination and with the cell operating at 25°C).[30] However, what matters in the present analysis is that these operational losses are also dependent on temperature.[18] Detailed balance analyses provide expressions of current and voltage losses and exhibit, at least, a linear dependence on cell temperature.[1,30,31] In general, since cell performances are assessed in the so-called STCs, their sensitivity to temperature is rated with respect to them with a temperature coefficient.[18] This coefficient assumes that the performance parameter (open-circuit voltage, short-circuit current, power at the maximum power point, conversion efficiency) varies linearly between the reference temperature (25°C) and the larger operating temperature. Hence, if these temperature coefficients make sense for temperatures not too different from 25°C, then they are less relevant for cells under thermal stress operating at temperatures ranging from 100°C to around 450°C. The core meaning of this statement is that it seems more appropriate to estimate the fundamental and operational losses at the functioning temperature than their variations with respect to those at 25°C.

Notwithstanding this, general trends valid for small temperature differences can be useful for analyzing the existing solar cells that were tested in the laboratory at temperatures >100°C. Details about these trends are not given in the text following, since they are available elsewhere.[1,18] First, it is well known that the efficiency drop with temperature is largely governed by that of the open-circuit voltage, in which generation and recombination rates annihilate each other. In the field, the thermal stress is mainly caused by an illumination >1 sun, meaning that the cell is

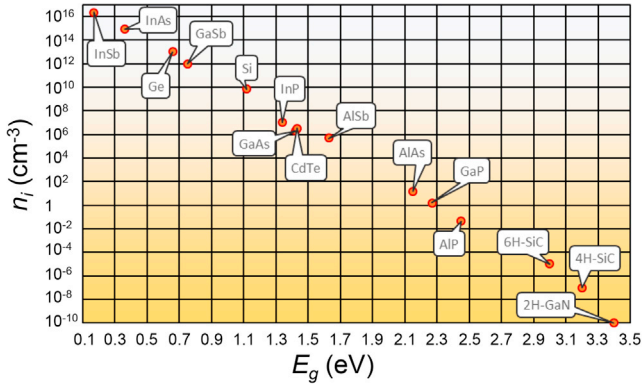


**Figure 3. Intrinsic Carrier Concentration of Mainstream Pure and Binary Alloy Semiconductors at 300 K**

Data from Piprek[34] and Hassan et al.[35] for SiC and GaN, respectively.

under solar concentrating conditions. One advantage is that the open-circuit voltage logarithmically rises with the concentration factor.[32] Hence, the decrease in open-circuit voltage caused by a growing recombination rate with temperature is somehow counter-balanced by the increasing generation rate provided by concentration. Second, in the frame of the single diode model, it is known that the dark saturation current sensitivity to temperature also plays a major role in the decrease of the open-circuit voltage.[1] Even though multiple recombination scenarios are possible (radiative, Auger, Shockley-Read-Hall, surface), the recombination current is roughly proportional to the intrinsic carrier density.[33] As a result, the intrinsic carrier concentration of semiconductors and its temperature dependence are major parameters to consider for making solar cells operational at high temperatures. Figure 3 shows that the intrinsic carrier concentration of semiconductors is a decreasing function of bandgap. Even though this concentration rises slightly more with temperature as the bandgap increases (in $\exp(-2E_g/(kT))$, where $k$ is the Boltzmann constant and $T$ is the cell temperature), the higher the operating temperature, the larger the bandgap needs to be. An elementary analysis based on stating that a cell becomes unusable when the intrinsic carrier concentration exceeds $10^{15}$ cm$^{-3}$ provides a temperature threshold above which survivability of the cell is compromised.[2] This limit is ~200°C for Si, ~350°C for GaAs (below this value for InGaAs ternary alloys), and between ~300°C and ~800°C for InGaP and AlGaAs ternary alloys.[2] However, if high-bandgap materials are required for solar cells under thermal stress, this is at the expense of current and, consequently, of efficiency, which both collapse due to the reduced collection of the solar spectrum for electrical power generation (see Figure 2).

For temperatures not too much above ambient, the dependence on temperature of the short-circuit current and the fill factor is less of a concern than that of the open-circuit voltage. Except for some perovskites, the bandgap of semiconductors decreases with temperature, and thus it is generally expected that the short-circuit current follows the opposite trend.[18] However, it should be remembered that external quantum efficiency varies with temperature,[36] as the result of changes in optical and electrical properties. In the case of solar cells under thermal stress, it has been previously shown that, on the one hand, concentration is required for raising the temperature, thus increasing current, but on the other hand, wide bandgaps are recommended to withstand high temperatures, thus decreasing current. Hence, the short-circuit current of solar cells that would be designed for operating in the field under

thermal stress, seems to depend on factors having opposite effects. Finally, the current level has a direct impact on the series resistance losses and thus on the fill factor. By considering the case in which resistance losses are negligible, the fill factor (generally noted $FF_0$) is favored by large bandgaps, while high temperature is detrimental.[37] Much less clear are the variations with temperature of shunt and, more important, series (at the contacts, in the metallic grid) electrical resistances,[18,36] and which temperature levels can be withstood without degradation[2]. Finally, the case of junctions connected in series is more complex to deal with because the current limiting sub-cell may change with temperature,[38] meaning that defining the architecture (bandgap, thicknesses of sub-cells) cannot obviously be optimum over a wide temperature range.

After this overview on sensitivity to the temperature of solar cells, it can be concluded that a lot of temperature-dependent physical parameters are involved, and predicting performances at high temperatures is definitely not a simple task. General trends can be identified, even though they sometimes have opposite effects. In this context, the next section describes the materials and architectures of solar cells that were tested in the laboratory at temperatures >100°C.

## MATERIALS

In Table 1, a list of selected solar cells tested in laboratory conditions under thermal stress is provided. The first column enumerates 12 single-junction cells with decreasing bandgap values, 1 double-, and 3 triple-junction cells. The test temperatures or temperature ranges, given in the second column, usually vary from room temperature (RT: 25°C) up to a maximum of 600°C (1 case), and mostly <400°C. For 6 of the 16 cases, the illumination is without concentration as shown in the third column. It is worth noticing that in cases with concentrated illumination, the concentration factors are moderate (<300), except in 4 cases, where they reach up to 1,000 and 1,500. It is very important to be aware that the tests are with both the cell temperature ($T$) and the concentration factor ($X$) controlled in the experimental setups. Hence, comprehensive analyses can be carried out. However, in real conditions, the cell temperature is a result of the illumination and thermal exchange operating conditions,[31] specific to each of the four applications identified in the first section (space missions or terrestrial hybrid systems, see Figure 1). This means that cases without any solar concentration and high testing temperatures are not in correspondence with any of the four applications mentioned above. Nevertheless, these particular cases still contribute to capitalizing knowledge on the behavior of these solar cells under thermal stress. In the following, the materials used for light absorption and charge generation, the front and back contacts, and the antireflection coatings (ARCs), are analyzed in detail. In particular, the effects of high operating temperatures (>100°C) on the properties critical for a proper functioning of the solar cells, are discussed.

### Semiconductor Materials and Cell Architectures

The high-bandgap single-junction cells (2.45–3 eV) are made of SiC[39] and GaN,[40-45] both appropriate for withstanding very high operating temperatures thanks to their very low intrinsic carrier concentration at 300 K (Figure 3). As already mentioned, such a choice is at the expense of conversion efficiency, which is only a few percent, especially for moderate concentration factors (see Figure 2B). Almost every cell in the table made of GaN is in fact a p-i-n GaN structure, in which the intrinsic layer is constituted of multiple quantum wells (MQWs) formed by alternating GaInN/GaN nanolayers, thus allowing bandgap tuning. The 5 single-junction solar cells with intermediate bandgap values (1.4–2 eV) are either made of (Al)InGaP[46-48,63]

**Table 1. Selected Solar Cells Tested in Laboratory Conditions under Thermal Stress (at Temperatures *T* above 100°C), without or with Concentration (Factor *X*)**

| Cell type | *T* (°C) | *X* | Compound ($E_g$ @ 300 K [eV]) | Substrate | ARC | Front and Back Contacts | Growth | Size | Ref. |
|---|---|---|---|---|---|---|---|---|---|
| Single | RT–275 | 1–150 | 6H-SiC (3.0) n on p and p on n | SiC | none | F: Ti/Al/Au/Pt; B: Au/Al | NS | 0.48 $cm^2$ | [39] |
| Single with MQW | RT–400 | 1–150 | GaN p-i-n with i-QW GaInN/GaN | sapphire | none | F: Ni/Au<br>B: Ti/Al/Ti/Au | MOVPE | 350 × 350 $\mu m^2$ | [40] |
| Single with MQW | RT–427 | 1 | GaN p-i-n with i-QW $Ga_{0.85}In_{0.15}N$/GaN | sapphire | ITO | F: Ti/Al/Ni/Au<br>B: NS | MOCVD | 1 × 1 $mm^2$ | [41] |
| Single with MQW | (‡) RT–500<br>(*) RT–600 | 1; 300 | GaN p on n with i-QW GaInN/GaN (2.75–2.95) | sapphire | ITO | F: Ti/Pt/Au<br>B: Ti/Al/Ni/Au | MOCVD | 2.5 × 2.5 $mm^2$ | (‡) [42]<br>(*) [43] |
| Single with MQW | 400, 450, 500* | 1 | GaN p-i-n with i-QW $Ga_{0.84}In_{0.16}N$/GaN | sapphire | ITO | F: Pd/Ni/Au<br>B: Ti/Al/Ni/Au | MOCVD | 1 × 1 $mm^2$ | [44] |
| Single with MQW | RT–500 | 1 | GaN p-i-n with i-QW GaInN/GaN (2.45–2.85) | GaN | none | NS | MOCVD | NS | [45] |
| Single | 25–400 | (‡) 1; 30–1,500<br>(*) 500* | (Al)GaInP (1.9, 2.0) n on p | GaAs | (‡) none; (*) $Al_2O_3$ encapsulation layer | (‡) F: Ti/WTi/Al/Ti<br>(*) F: Ti/Pt/Al/Pt; (*) B: Au* | MOVPE | 0.1 $cm^2$ | (‡)[46] (+[47])<br>(*)[48] |
| Single | −70 to 125 | 1–150 | GaAs (1.42) | GaAs | $Ta_2O_5/MgF_2$ | NS | NS | NS | [49] (+[50]) |
| Single | RT–450 | 1 | GaAs (1.42) | GaAs | none | NS | MOCVD | 1 $cm^2$ | [51] |
| Single | 25–400 | (‡) 1; 30–1,500<br>(*) 500* | GaAs (1.42) n on p | GaAs | (‡) none ; (*) $Al_2O_3$ encapsulation layer | F: Au/Pt/Al/Pt/Ti ; (*) B: Au* | MOVPE | 0.1 $cm^2$ | (‡)[46]<br>(*)[48] |
| Single | RT–500 | 1* | GaAs (1.42) | GaAs | $TiO_x/Al_2O_3$ | NS | MBE | 30.53 $mm^2$ | [52] |
| Single | RT–250 | 1 | (Al)GaSb (0.72, 0.88, 1.30) | GaSb | none | F: Ti/Pt/Au<br>B: Ni/Ge/Au/Pt/Au | MBE | 0.5 × 0.5 $cm^2$ | [53] |
| Double | RT–400 | (‡) 1; 300–1,000<br>(*)(*) 1; 20–1,500* | (Al)GaInP (2.0)/GaAs (1.42) | GaAs | (*)(*) $TiO_2/Al_2O_3$ (*) ZnS/$MgF_2$ or $Ta_2O_5$/$MgF_2$;(‡) yes (NS) | (‡)(*)(*)F: Ti/Pt/Al/Pt<br>or (*) F: Ti/WTi/Ag/Ti*<br>or (*) F: Au; (*) B: Au | MOVPE | NS | (‡)[54]<br>(*)[55]<br>(*)[56] |
| Triple | 30–240 | 1–14 | $In_{0.49}Ga_{0.51}P$ (1.86)/$In_{0.01}Ga_{0.99}As$ (1.40)/Ge (0.65) | Ge | yes (NS) | F: n-GaAs/Ag*<br>B: Ag | MOCVD | 1 $cm^2$ | [57] |
| Triple | RT–125 | 1–1,000 | GaInP (1.8)/GaAs (1.4)/InGaAs (1.0) | GaAs (removed) | ZnS/$MgF_2$ | F: Se-doped GaInNAs/Au<br>B: Au | MOVPE | 0.1 $cm^2$ | [58] (+[59,60]) |
| Triple | 50, 100, 150, 180, 230 | 1; 8 (rem: AM0) | GaInP/GaAs (1.42)/Ge (0.65) | NS | $MgF_2$ (+ cover glass, UV cutoff) | NS | NS | 40 × 37.72 $mm^2$ | [61] (+[62]) |

Main parameters in terms of materials (architecture, substrate, antireflection coating layers, front and back contact layers), layer deposition technique, and size. ITO, indium tin oxide; LPE, liquid phase epitaxy; MBE, molecular beam epitaxy; MOVPE or MOCVD, metalorganic vapor-phase epitaxy-metalorganic chemical vapor deposition; NS, not specified; MQW, multiple quantum wells; RT, room temperature; UV, ultraviolet.

or GaAs.[46,48-50,52] It is worth noticing that GaAs seems to be an optimal choice for temperatures : 150°C–200°C (Figure 2B), hence, for hybrid PV-T and PV-TE systems. Since InGaP is capable of withstanding temperatures >350°C[2], it seems to be appropriate for hybrid PV-CSP systems. By tuning the In-Ga composition, a thermal breakdown can be avoided while minimizing the efficiency drop expected for bandgaps >1.4 eV at 500°C, even if concentration factors are >100 (see Zeitouny et al.,[28] in which the SQ efficiency limit is calculated for $X$ = 1,000). The next case down in the table is a GaSb cell ($E_g$ = 0.72 eV at 300 K). A low bandgap being a major handicap for high temperatures, Al is added to reach higher bandgap values (up to 1.3 eV).[53] There is only one dual-junction cell, made of a stack of (Al)GaInP (2 eV) on GaAs (1.42 eV) and tested at temperatures ranging from RT to 400°C, without or with concentrations up to $X$ = 1,500.[54-56] The listed 3 triple-junction cells are made of InGaP/InGaAs/Ge[57] and InGaP/GaAs/Ge[61] stacks designed for near-the-sun space missions ($T$ up to 240°C, $X$ up to 14), and 1 inverted metamorphic InGaP/GaAs/InGaAs architecture,[58,59] tested for CPVs under moderate thermal stress ($T$ up to 125°C, $X$ up to 1,000). It is interesting to note that Si, CIGS (copper indium gallium selenide), CdTe, and perovskite are not in the table. Even though Si is the mainstream PV technology, it is not appropriate at high temperature because of its high intrinsic carrier concentration (Figure 3) and non-optimal SQ efficiency compared to GaAs (Figure 2B). When the temperature rises, CIGS and CdTe solar cells seem to be subject to the migration of elements, causing shunt paths. Perovskite cells are probably not mature enough in the STC for being tested at high temperatures.

In Table 1, bandgaps at 300 K are provided. Their variations with temperature are critical, in particular for multi-junction cells, which require current matching. It is essential to note that material composition can change since thermal exposure may lead to (1) the diffusion of dopants,[64] inducing layer thickness variations and dopant mixing in the space charge region; (2) the decomposition and/or outgassing of volatile components of the semiconductor compounds.[2]

In the case of multi-junction solar cells, tunnel junctions (TJs) act as transparent and conductive structures to provide an ohmic interconnection between the sub-cells. A wealth of information about TJs is available in a review article by Colter et al.[65] In particular, the impact of annealing on TJs is addressed (bearing in mind that their optimum growth temperature is lower than that used for the rest of the multi-junction cell elements). Initially, the deterioration induced by a thermal exposure was attributed to dopant inter-diffusion at the junction. However, studies aiming at substituting fast diffusing dopants by slower diffusing ones remain inconclusive.[65] It would therefore indicate that inter-diffusion of dopants is not a major concern. The experimental results of multi-junction at high temperature do not exhibit any sign of limitation attributable to the TJ (any specific spike on the current-voltage ($I$-$V$) characteristic, as observed under concentrated light in Braun et al.[66] and Vossier et al.[67]). In addition, at high temperature, the sheet resistance of the top layer depends on its composition.[55] In the following, the performance of contacts under thermal stress is discussed in detail.

## Contacts

A high-performance electrical contact at a metal-semiconductor junction should allow the flow of electrical charges while minimizing the voltage drop. In other words, it requires a non-rectifying low-resistive interface. The potential barrier at this interface is usually described by the Schottky model.[68] According to this theory, the barrier height depends on the semiconductor electron affinity and the metal

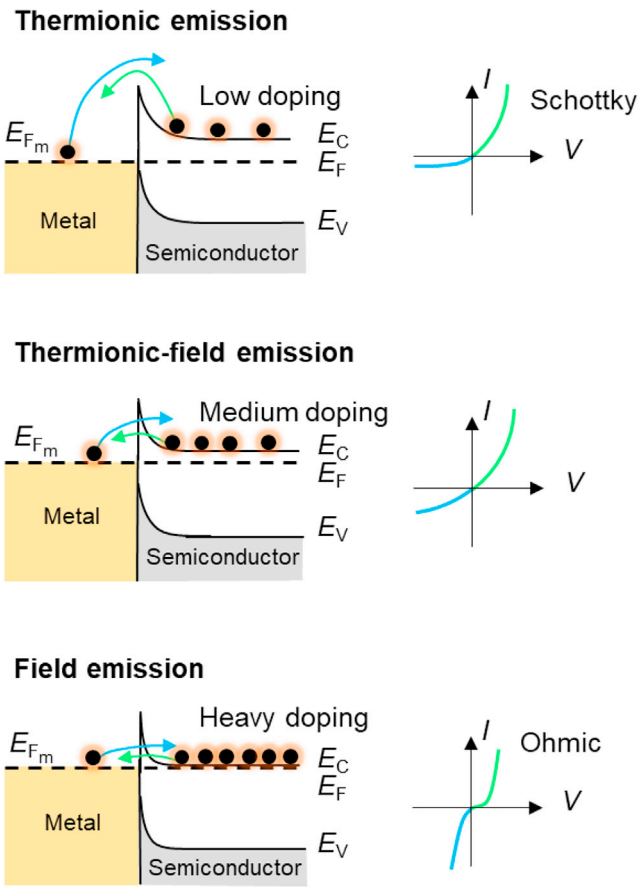


**Figure 4. Conduction Mechanisms at the Metal-Semiconductor Interface as a Function of the Doping Level, and Their I-V Characteristics**
Adapted from Schroder[68] and Sze & Ng[76].

work function. Although accumulation- or neutral-type contacts are preferred, a depletion-type contact is generally formed. The barrier height is relatively independent of the metal work function due to surface states at the interface. In practice, the barrier is modified by tuning the semiconductor doping level, which affects the barrier width. In the literature, the involved conduction mechanisms are classified according to the doping level. Thermionic emission, thermionic-field emission, and field emission mechanisms occur for low, medium, and heavy doping levels, respectively. These mechanisms and their *I-V* characteristics are illustrated in Figure 4. The previously mentioned mechanism is the most favorable, as it provides an ohmic contact with a linear and sharp *I-V* characteristic at about $V = 0$ V, which corresponds to a low specific contact resistivity. For each conduction mechanism, the specific contact resistivity can be described by empirical equations that depend on temperature.[68] However, this temperature dependence usually has a simple form because the specific contact resistivity is much more dependent on the doping level and surface states. For temperatures >300 K, the temperature dependence cannot be generalized and thus must be evaluated on a case-by-case basis from experiments.

Furthermore, the experimental results on (Al)GaInP/GaAs tandem cells[55] show that minimization of the specific contact resistivity is not sufficient. They indicate that the sheet resistance increases with temperature and becomes detrimental to the cell performance (particularly the voltage at the maximum power point) at high

temperature (300°C–400°C). Joule losses are known to decrease cell performances under solar concentration. This is because they are proportional to the series resistance of the device and the current squared. For this reason, each contribution to the series resistance must be minimized for high-temperature operating conditions. The tradeoff between the lateral resistance and the grid shadowing must be reassessed. For a fine optimization of the grid shape, a 3-dimensional distributed electrical circuit modeling[69] can be used. This model is applicable to single- and multi-junction solar cells.[70] Thus far, the temperature dependence is accounted for in the model of each diode, but not for the network of resistances.

For high-temperature operating conditions, the stability of contacts is crucial. The metals used for the contacts should have a melting point temperature that is higher than the operating temperature. Under thermal stress, metals can diffuse or form alloys with semiconductors, leading to permanent damage caused by a shunting of the junction.[2] Refractory metals are known for being extremely resistant to temperature. A few articles report on the use of refractory metals for solar cells, mainly made of tungsten alloys (WN or WTi), that are conductive and act as a barrier to prevent interactions with the underlying semiconductor.[55,63] However, refractory metals are not mandatory, since standard metals (Ag, Al, Au, Ni, Pd, Pt, and Ti), already used for solar cells put under thermal stress, have a high melting point (>660°C). Experimental assessments at temperatures up to 450°C of solar cells with contacts made of those standard metals are reported in Table 1. Details about the metallization contacts are provided in the seventh column. It can be noted that when a stack of 4 metallic layers (Ti/Pt/Al/Pt) for the n-type contact and an Au layer for the p-type contact are used, cell performance is stable up to 450°C. In this particular case, compared to common metal stacks reported for CPV applications, an additional layer (of Pt or Ti) is deposited on the top to prevent the underlying Al layer from oxidizing.

### ARCs

Under thermal stress, stability of the ARC is another main concern. A very limited number of studies report on this matter (see the sixth column in Table 1). Thanks to a good stability up to 600°C, indium tin oxide (ITO), deposited by reactive e-beam evaporation and post-annealed in dry air at 500°C, is used for the GaN cells.[41-44] Interestingly, three bilayers were investigated by Steiner et al.[56]: ZnS/$MgF_2$, $Ta_2O_5$/$MgF_2$, and $TiO_2$/$Al_2O_3$. Cell performances decline significantly at 400°C with the ZnS/$MgF_2$ and $Ta_2O_5$/$MgF_2$ bilayers, whereas the $TiO_2$/$Al_2O_3$ coating is stable. However, the $TiO_2$/$Al_2O_3$ bilayer is the source of parasitic absorption at short wavelengths under high-temperature operating conditions.[55]

## PERFORMANCE

### Testing Procedures

Standard solar cell testing procedures consist of measuring the *I-V* characteristics under dark and 1-sun illumination conditions and the external quantum efficiency (EQE). In the so-called STCs, the cell temperature is kept at 25°C, typically by using a Peltier module. For larger temperatures, particularly >100°C, a more sophisticated control of the cell temperature and its environment is required. The use of a HFS600E-PB4 temperature-controlled stage, from Linkam Scientific Instruments, is systematically reported in the literature. This stage allows us to perform electro-optical measurements on cells whose temperature is controlled from 25°C to 600°C in a $N_2$ environment (to prevent oxidation).[46] It is worth noting that reflection and absorption by the stage window must be considered in the data processing.

Measuring the efficiency of multi-junction cells operating at high temperature is a sensitive task due to the bandgap shift of the sub-cells and intensity spikes in the lamp spectrum.[54] The spectrum of the solar simulator must be adjusted at each temperature in conjunction with the external quantum efficiency curves and calibrated reference photodiodes. Additional lamps, typically brightness-adjustable light-emitting diodes (LEDs), are used for this purpose. More details on this calibration procedure are available in Steiner et al.[58] For the measurements under light concentration, a flash lamp is commonly used to avoid the self-heating of cells. This type of lamp allows better control of the cell temperature. However, the spectrum adjustment remains a challenge, as it can induce a significant error in the evaluation of the fill factor.[54]

The measurement of quantum efficiency also requires special care in the case of multi-junction solar cells. The sub-cells, usually connected in series, must be tested under short-circuit conditions. To do so, light biasing is used to ensure that the sub-cell under test delivers the lowest current. In addition, a voltage bias is applied to counterbalance the ones produced by the non-tested sub-cells (illuminated in the optical bias conditions). Detailed procedures and typical measurement artifacts for tandem and triple-junction solar cells are described by Burdick and Glatfelter[71] and Meusel et al.,[72] respectively. It is worth noting that the light and voltage biases must be readjusted at each temperature.

### Performance Analysis for SiC and GaInN/GaN Cells

The case of 6H-SiC cells[39] is very specific because of the large bandgap (3 eV at 300 K, still 2.96 eV at 275°C, the largest tested temperature). It follows from SQ efficiency limit calculations as a function of temperature and concentration factor (see examples in Figure 2) that a maximum efficiency of a few percent can be hardly expected. Unfortunately, for these first-ever fabricated SiC solar cells, the best value is <0.25% at 25°C and $X \sim 150$, partially explained by a fill factor <0.5 (50%). Better performances are awaited with the GaInN/GaN MQW cells, owing to the possible bandgap tuning down to 2.45 eV.[43,45] This is indeed the case, with a measured efficiency of 1.9% at RT, decreasing to 0.4% at 600°C under 1-sun illumination in the work described by Williams et al.[43] Figure 5 shows an analysis of the experimental data versus the SQ efficiency limit calculated for each tested temperature. It is striking to observe that since the measured bandgap decreases from 2.88 eV at 25°C to 2.64 eV at 600°C, the SQ efficiency is almost unchanged (the drop is only an absolute −0.3%, from 6.1% to 5.8%). However, for the measured efficiencies, the drop is an absolute −1.5%, but from 1.9% at 25°C (31.4% of the SQ limit) down to 0.4% (only 6.9% of the SQ limit). This means that if luckily the absorber material bandgap changes in such a way that the ideal efficiency remains almost the same, the performance of the fabricated cell further deviates from the optimal one when the temperature increases. The causes of such deviations are multiple (Temperature Sensitivity of Solar Cells in a Nutshell) and are usually investigated by analyzing additional experimental data, such as the EQE, and the typical figures of merit: short-circuit current ($J_{sc}$), open-circuit voltage, and fill factor values extracted from the *I-V* curves. In the case of GaInN/GaN MQW cells, as the temperature increases, these are large leakage currents in reverse bias in the dark and smaller series resistances,[45] EQE drops at small wavelengths possibly due to filtering by the top p-doped GaN layers,[43] while performance stability is observed under thermal stress in Huang et al.[44] It is worth mentioning other measurements on GaInN/GaN MQW cells showing slight efficiency improvements, from 0.46% (25°C) to 0.59% (250°C) in Zhao et al.[40], and from 0.6% (26.9°C) to 1.5% (376.9°C) in Lien et al.,[41] and then it drops at higher temperatures. Interestingly, these improvements are somehow

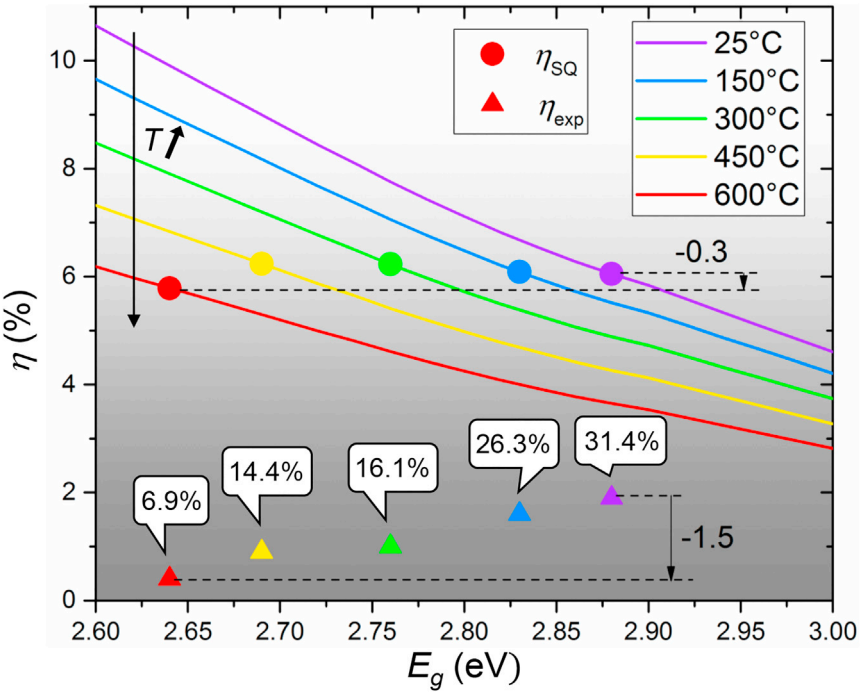


**Figure 5. Analysis of the Efficiency of InGaN/GaN Multiple Quantum Well Solar Cells Tested under 1-Sun Illumination as a Function of Temperature**

Data from Williams et al.[43] The lines are the SQ maximum efficiencies calculated for each of the tested temperatures. The circles are the SQ efficiencies calculated at the bandgaps experimentally determined at each temperature. The triangles are the measured efficiencies. The percentages indicate the fraction of the SQ efficiency reached by the tested cell.

predicted by SQ calculations for large bandgaps (see Figure 2B for GaN and Figure 5), especially when the bandgap reduction with temperature is substantial. However, as already stated multiple times, with these high-bandgap (>2.5 eV) cells, the efficiency is not optimal because of current limitations, even under concentration (see, e.g., Zeitouny et al.[28]).

## Performance Analysis for (Al)GaInP and GaAs Cells

Better performances are expected with the 6 single-junction solar cells with intermediate bandgap values (1.4–2 eV) either made of (Al)GaInP[46-48,63] or GaAs.[46,48-50,52] The analysis focuses first on the open-circuit voltage since it is the figure of merit that is the most sensitive to temperature (Temperature Sensitivity of Solar Cells in a Nutshell). A specific reading grid, mixing ideas given in articles about the fundamental losses of solar cells by Hirst and Ekins-Daukes,[22] the additional losses and their variations with temperature by Dupré et al.,[18] and the use of the SQ limit by Guillemoles et al.[21] for analyzing the performances of solar cells, as in the article by Nayak et al.,[30] is proposed hereafter. The main point is that if it is assumed that the solar spectrum is that of a blackbody at temperature $T_s$ and using Boltzmann's approximation of the Planck functions, then the open-circuit voltage of a solar cell at temperature $T$ operating in the SQ limit ($V_{oc}^{SQ}$) can be calculated using[22]

$$qV_{oc}^{SQ}(T,X) = E_g(T)\left(1-\frac{T}{T_s}\right) + kTln\left(\frac{\Omega_{abs}(X)}{\Omega_{emit}}\right) + kTln\left(\frac{\gamma(E_g(T),T_s)}{\gamma(E_g(T),T)}\right) \quad \text{(Equation 1)}$$

where $\Omega_{abs}$ and $\Omega_{emit}$ are the projected absorption and emission solid angles (with $\Omega_{abs}(X) = X\Omega_{abs}$) and $\gamma(E,T) = (2kT/(c^2h^3))(E^2 + 2kTE + 2k^2T^2)$. The dependence of

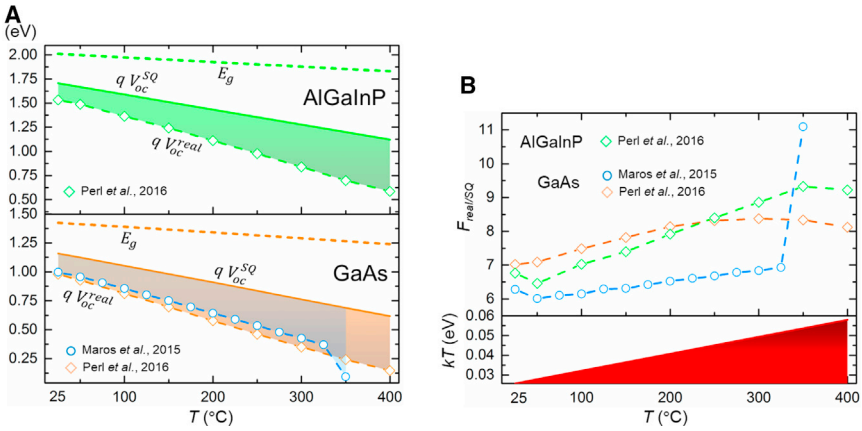


**Figure 6. Analysis of the Open-Circuit Voltage of AlGaInP ($E_g$ = 2 eV at 300 K) and GaAs ($E_g$ = 1.4 eV at 300 K) Solar Cells Tested under Thermal Stress without Any Concentration ($X$ = 1)**

Variations of $E_g$, $V_{oc}^{SQ}$, and $V_{oc}^{real}$ (A) and of $F_{real/SQ}$ (B) as a function of cell temperature (experimental data from Perl et al.[46] and Maros et al.[51]). Sensitivity of the bandgap to temperature is calculated using Varshni's relation[27] with parameters from Vurgaftman et al.[26] for GaAs, and assuming linear variations between the measured values (2.01 eV at 25°C, 1.83 eV at 400°C[46]) for the AlGaInP cell. $V_{oc}^{SQ}$ is calculated using the AM 1.5 D solar spectrum to match the experimental conditions.

the bandgap on temperature as well as the dependence of the absorption projected solid angle on the concentration factor ($X$), required in the present analysis of solar cells operating in HIHT conditions, are accounted for. In real conditions, multiple losses must be added to these fundamental losses in such a way that the deviation of the open-circuit voltage of the cell operating in real conditions ($V_{oc}^{real}$) can be written as a reformulation of the equations in Guillemoles et al.[21] and Nayak et al.,[30] as follows:

$$q\left[V_{oc}^{SQ}(T,X) - V_{oc}^{real}(T,X)\right] = kT\ ln(FM(T,X)) = kT \times F_{real/SQ} \qquad \text{(Equation 2)}$$

where the $kT$ multiplicative factor, $F_{real/SQ} = ln(FM(T,X))\ (\geq 0)$, can be expressed as the product of various figures of merit quantifying the deviations from the SQ assumptions,[21] such as non-ideal absorption of the useful photons, electron-hole pair generation and collection, the addition of non-radiative recombination, and resistance losses (see the details in Guillemoles et al.[21] and Nayak et al.[30]).

This simple expression indicates the "price" for the open-circuit voltage of increasing the operating temperature of the solar cells, which grows as $kT$ (26 meV at 25°C and 58 meV at 400°C, see Figure 6B), in addition to the "price" already paid in the SQ limit (this parameter is also proportional to the temperature of the cell, as Equation 1 shows). Hence, when the temperature rises, it becomes increasingly important to take up the challenge of minimizing as much as possible the multiplicative factor ($F_{real/SQ}$) representing the deviations from the ideal SQ limit.

In the following, the parameters $V_{oc}^{SQ}$, $V_{oc}^{real}$, and $F_{real/SQ}$ are used to analyze the performance of AlGaInP and GaAs solar cells tested at high temperature. $V_{oc}^{SQ}$ is calculated properly for the solar spectrum (AM 1.5 D) corresponding to the experiments and in place of the blackbody distribution used in the previous analysis. The factor $F_{real/SQ}$, showing how many $kT$ ($kT/q$, where $q$ is the elementary charge) away $qV_{oc}^{real}$ ($V_{oc}^{real}$) is from $qV_{oc}^{SQ}$ ($V_{oc}^{SQ}$), allows a fair comparison in different operating conditions ($T$ and $X$). Figure 6A shows the results for 3 cells, 1 made of AlGaInP[46] and 2 made of GaAs,[46,51] as a function of temperature without any concentration

($X$ = 1). The first and often overlooked cause of open-circuit voltage drops is the bandgap reduction. The benefit of this decrease to the short-circuit current is generally emphasized, but $E_g/q$ is the value from which open-circuit voltage losses pile up (see Equation 1). The SQ open-circuit voltage declines as expected (−0.59 V, from 1.71 V at 25°C to 1.12 V at 400°C for the AlGaInP cell) because the balance between generation and recombination is driven by increased emission with temperature. The measured values are below, with a larger decline (−0.94 V from 25°C to 400°C) because of the additional losses. The plot suggests that the difference between $V_{oc}^{SQ}$ and $V_{oc}^{real}$ is constantly proportional to $kT$, but Figure 6B indicates that this is not the case. The factor $F_{real/SQ}$ varies between 6.8 and 9.2, with the minimum at 50°C and the maximum at 350°C. Comparatively, the open-circuit voltage of one of the GaAs cells is similar ($7.0 \leq F_{real/SQ} \leq 8.1$), while the open-circuit voltage of the other is a little bit closer to the SQ limit ($6.3 \leq F_{real/SQ} \leq 11.1$), except at 350°C, where a voltage drop takes place. This analysis demonstrates that all of these cells follow the expected decline trend, but the non-fundamental voltage losses (non-radiative recombination) obviously become worse as temperature rises.

The same analysis is made by adding the impact of concentration (Figure 7). Concentration lowers the mismatch between absorption and emission solid angles. As a consequence, the SQ open-circuit voltage increases as $ln(X)$. The open-circuit voltage of the tested AlGaInP and GaAs cells follows this trend. However, other effects are taking place since the factor quantifying the deviation from the real to the SQ open-circuit voltage is not constant with the concentration factor. For the AlGaInP cell, there is an optimum at around $X$ = 150 for all tested temperatures, except at 400°C (temperature at which $F_{real/SQ}$ keeps increasing with $X$). Interestingly, this is quite different for the GaAs cell, whose open-circuit voltage gets closer to the SQ value when the concentration factor increases, until a floor value of $F_{real/SQ}$ of around 4.7 is reached for $X > 100$ at all temperatures.

To understand the mechanisms responsible for these behaviors, device analyses can be performed, using technology computer-aided design (TCAD) simulations[50] or diode models.[48] One critical point is the physical parameters, and in particular the temperature dependence of the intrinsic carrier concentrations and minority carrier lifetimes that play a central role in open-circuit voltage variations. Time-resolved photoluminescence measurements made on GaAs, GaInP, and AlGaInP samples in the temperature range 25°C–400°C exhibit opposite trends for GaAs (the effective lifetime, dominated by radiative recombination, increases with temperature) and (Al)GaInP (the effective lifetime, dominated by thermionic emission, decreases with temperature). Hence, lifetime sensitivity to temperature must be considered for better understanding the experimental data and proposing cell-design improvements.

The effects of thermal stress on the short-circuit current are less critical, as expected. Every internal quantum efficiency (IQE) and EQE measurements made on the AlGaInP and GaAs cells exhibit a stability with temperature on the spectral range where the values are maximum, up to 300°C–350°C[51] and 400°C.[46] In each case, bandgap reduction caused by a temperature elevation is observed for the absorber and emitter layer materials, and for the window layer materials (AlInP and GaInP).[46,51,52] All in all, the short-circuit current is an increasing function of temperature, with drops greater than around 300°C for the cells in Maros et al.[51] Even though gauging the experimental values ($J_{sc}^{real}$) against the maximum SQ values ($J_{sc}^{SQ}$) is disadvantageous for the cells without ARC, it is worth noticing a stable value

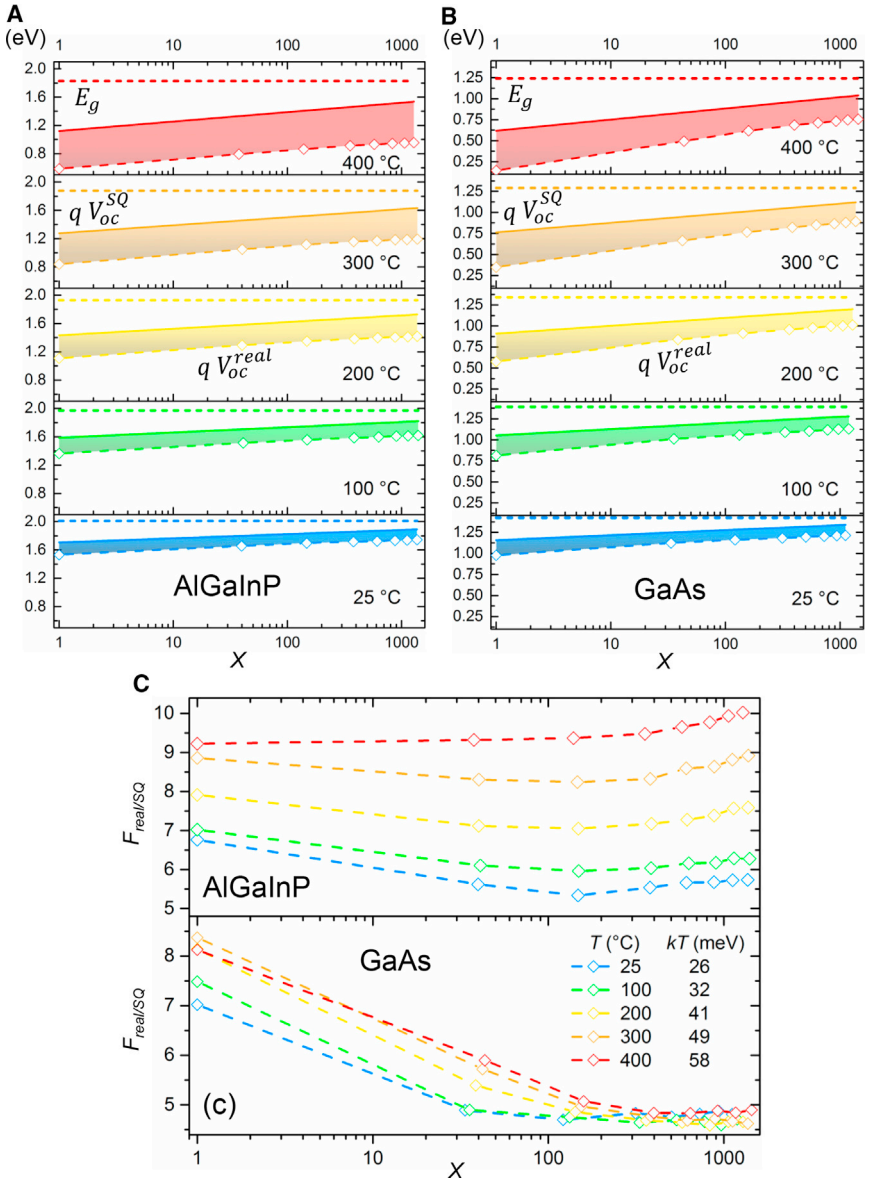


**Figure 7. Analysis of the Open-Circuit Voltage of AlGaInP ($E_g$ = 2 eV at 300 K) and GaAs ($E_g$ = 1.4 eV at 300 K) Solar Cells Tested under Thermal Stress without or with Concentration**

Variations as a function of cell temperature: of $E_g$, $V_{oc}^{SQ}$, and $V_{oc}^{real}$ (A) for an AlGaInP cell, (B) a GaAs cell, and (C) of $F_{real/SQ}$. Experimental data from Perl et al.[46] Sensitivity of the bandgaps to temperature and $V_{oc}^{SQ}$ are calculated as in Figure 6.

of around 0.44 (0.74) for the ratio $J_{sc}^{real}/J_{sc}^{SQ}$ from RT to 400°C (300°C–350°C) for the GaAs cells in Perl et al.[46] and Maros et al.[51], and of around 0.62 from RT to 400°C for the AlGaInP cell in Perl et al.[46] ($X = 1$, $V_{oc}$ analyzed in Figure 6). For the GaAs cells in Maros et al.,[51] this is not the same for the ratio of the fill factors $FF^{real}/FF^{SQ}$, which declines linearly from 0.84 (0.75/0.90) at RT down to 0.54 (0.41/0.76) at 325°C (before dropping down to 0.36 at 350°C). However, this trend is chiefly caused by the degradation of the open-circuit voltage. The additional impact of series resistance is visible in the case of GaAs cells subjected to a laser beam for analyzing the impact of high optical injection. As a matter of fact, if the fill factor increases

with the open-circuit voltage up to a maximum reached at a current density of around 5 to 6 A $cm^{-2}$, then a slight decline follows.[52] The same article also shows stable performances after annealing the cells at 400°C or 450°C for 200 h. Finally, since analyses in the articles focus more on understanding the physics than on performance per se, conversion efficiency is not necessarily studied closely, and thus there is not enough material to draw fully meaningful conclusions.

### Performance Analysis for (Al)GaSb Cells

The GaSb cells with the lower bandgap (0.72 at 300 K) cannot survive temperatures >200°C,[53] as anticipated. The open-circuit voltage drops from 0.275 V at RT to 0.035 V at 175°C. Contrary to usual, the short-circuit current decreases with temperature. This is probably because, when temperature rises, the window layer (AlAsSb) filters out photons and acts as a diffusion barrier to minority carriers. Variations with temperature of the shunt and series resistances help to understand the deviations from the resistance-free fill factor only driven by the ratio of the open-circuit voltage to temperature ($qV_{oc}/kT$). As expected, with the adjunction of Al and the resulting larger bandgaps (up to 1.3 eV at 300 K), the AlGASb cells withstand higher temperatures. Performances above 100°C are better than those of the GaSb cell despite the handicap of a smaller RT short-circuit current, which is caused by the transition from direct to indirect bandgap material, not counteracted by thickening the absorber.

### Performance Analysis for Multi-junction Cells

The case of the (Al)GaInP/GaAs dual-junction cell is different from all of the previous ones because of the choice to design the cell for optimal operation at high temperature (400°C) and high illumination ($X = 1{,}000$). This approach makes particular sense at least to ensure current matching between the two sub-cells at the targeted high temperature. A remarkable result is the inversion in hierarchy in terms of open-circuit voltage for the AlGaInP cells with different Al contents (from 0% to 12%), under concentration ($X \sim 1{,}000$). At room temperature, the cell with the highest Al contents has the largest open-circuit voltage. According to the usual temperature coefficient theories, the higher the open-circuit voltage (bandgap), the lower its temperature coefficient.[18] This statement is correct provided that the mechanisms driving the temperature sensitivity of the open-circuit voltage remain the same over the temperature range of interest. It is not the case for the AlGaInP cells tested by Perl et al.[55] at temperatures beyond the usual limits: at ≥300°C, this is the cell without Al that has the largest open-circuit voltage. This important result is consistent with the change in $F_{real/SQ}$ with temperature observed in Figures 6 and 7, meaning that perfect linear variations of the open-circuit voltage are quite unlikely over extended temperature ranges. This validates the statement made in Temperature Sensitivity of Solar Cells in a Nutshell that temperature coefficient analyses are questionable beyond a reasonable temperature span.

Hence, GaInP is more appropriate as the top cell,[55] which is the current-limiting subcell at RT. However, its short-circuit current increases more with temperature than that of the GaAs bottom cell, in such a way that current matching is reached at around 300°C. The trapezoid-shaped EQE has a stable maximum with temperature, while shifting toward longer wavelengths. If the cause of this shift is the decreasing bandgap for all epitaxially grown materials, the low-wavelength side redshift of the EQE for the InGaP top cell would be due to a temperature-sensitive absorption of the $TiO_2/Al_2O_3$ ARC. The faster increase with temperature of the sheet resistance for AlGaInP cells argues once again for the use of a GaInP top cell. In addition, by considering that the Al grid resistance doubles from RT to 400°C, it makes sense that the fill factor declines with temperature and also above a temperature-

dependent optimum concentration factor. With these trends for the short-circuit current and fill factor, and the open-circuit voltage varying as $ln(X)$ and dropping with temperature, all in all this dual-junction cell withstands high temperatures, but at the cost of efficiency losses, from 30.3% to 16.2% with optimum concentration (25.4% down to 5.9% without concentration) when the temperature rises from 25°C to 400°C.

In the case of the InGaP/InGaAs/Ge triple-junction cell,[57] the results show once again that the slope of the open-circuit voltage decline with temperature is different under thermal stress (170°C–240°C) from that in the lower temperature range (30°C–100°C). Since the Ge bottom cell has a very low bandgap (0.65 eV at 300 K) and intrinsic carrier concentration (see Figure 3), the open-circuit voltage drop with temperature (up to 240°C) must be counteracted by concentrating sunlight (up to $X = 14$, AM1.5 G spectrum). The GaInP/GaAs/Ge triple-junction cell[61] withstands 280°C under concentration ($X = 8$, AM0 spectrum). Interestingly, the way the short-circuit current depends on the angle of incidence, to be considered for space missions, varies with temperature.[62] It is worth mentioning that annealing of this triple-junction cell for dozens of hours at temperatures from 150°C to 230°C leads to recoveries of the open-circuit voltage and the short-circuit current after damaging caused by electron irradiation.[61] The Ge-free GaInP/GaAs/InGaAs inverted metamorphic multi-junction is expected to be less sensitive to temperature than the aforementioned triple-junction cells having a Ge bottom cell,[58] due to the higher InGaAs bandgap (1.0 eV at 300 K). Tested at a maximum temperature of 126.1°C, the efficiency of this cell is still 33.8%, with an optimum concentration factor of 460. A key point is that current in each sub-cell varies with temperature, possibly in different ways, thus leading to changes in which of them is limiting.[1] In particular, the optimum bandgaps for the middle and bottom cells must be selected considering the atmospheric absorption bands in the solar spectrum, by avoiding that the bandgap shift does not fall in one of these bands when the temperature increases.[58]

### Efficiency Chart

The number of solar cells tested thus far at temperatures >100°C is fairly limited. Figure 8 provides an efficiency chart built with data (directly or from calculations using other data) only available in 10 of the 16 lines in Table 1. The lowest (<1.4 eV) and highest (>2eV) bandgap solar cells are characterized by a low efficiency (<3.2%). The GaInN/GaN MQW cells withstand the largest thermal stress and exhibit various and sometimes unusual temperature sensitivities. A very high concentration may help increase efficiency, but not by very much, according to SQ limit calculations (see Figure 2 and Zeitouny et al.[28]). Efficiency data for triple- and dual-junction cells, and single-junction cells with intermediate bandgap values (1.4–2 eV), are quite scarce for temperatures >100°C. The lines connecting the measurement data points, added as a guide for the eyes, may lead to the perception of perfectly straight lines connecting the points at both ends. However, the analyses proposed above have shown that over wide temperature ranges, many physical parameters affect the performances of solar cells in a way that is not just a simple linear dependence on temperature.

## DISCUSSION

Solar cells used for space missions close to the sun and in terrestrial hybrid systems involving solar-to-thermal energy conversion devices call for a better understanding of their behavior under thermal stress. There are simple primary guidelines for selecting the materials able to survive high temperatures. The semiconductor

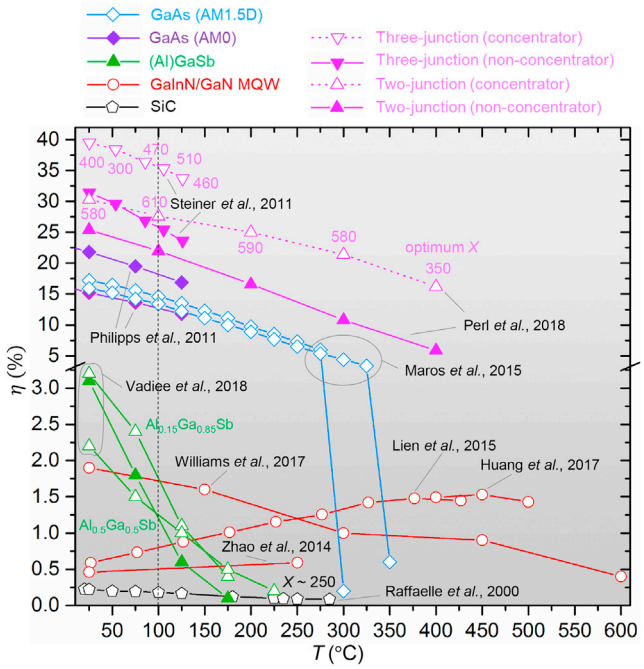


**Figure 8. Efficiency Chart for the Cells Tested under Thermal Stress Listed in Table 1**

Data from Raffaelle et al.[39] for the SiC; Zhao et al.,[40] Lien et al.,[41] Williams et al.,[43] and Huang et al.[44] for the GaInN/GaN MQW; Philipps et al.[49] and Maros et al.[51] for the GaAs; Vadiee et al.[53] for the (Al)GaSb; Perl et al.[55] for the 2J InGaP/GaAs; and Steiner et al.[58] for the 3J GaInP/GaAs/GaInAs solar cells (efficiency explicitly provided or calculable from other data). Note the break in the vertical scale.

materials can be chosen by using an elementary criterion based on the intrinsic carrier concentration, and SQ efficiency limits calculations. Prior knowledge of the temperature sensitivity of electrical and optical properties is required for selecting the materials for the contacts and ARCs, respectively. Nevertheless, there are also a large number of other parameters that govern the behavior of solar cells under thermal stress in non-trivial ways.

Of course, the solar cells tested at high temperature in laboratory conditions suffer from multiple losses, in addition to those considered in the ideal SQ limit. The analysis performed in this article has revealed that evaluating the deviations from the SQ limit at each temperature is a fair method for comparing the performances of real cells at different temperatures. In particular, for the open-circuit voltage, gauging these deviations with a factor of $kT$ seems to be quite appropriate. In the same way, assuming linear temperature sensitivities of the open-circuit voltage, short-circuit current, and fill factor, and hence using temperature coefficients, make sense over a limited temperature range, but temperature coefficients seem to be inadequate for relating the figures of merit at two temperatures very different from each other.

The 16 cases of cells tested at temperatures >100°C and considered in the present article have revealed that a cell optimally designed at room temperature may not remain necessarily optimum at a much higher temperature. By way of illustration, a recent article reports on the design of solar cells for operating at high temperature in the lower atmosphere and at the surface of Venus where the temperature can reach 465°C.[73] The article clearly demonstrates that the optimum high-temperature cells differ in terms of their architecture, and sometimes in terms of their materials,

compared to those optimized in the standard test conditions (at 25°C). Sensitivity to temperature of each physical parameter governing the PV effect, from optical generation of electrical charges to their collection, must be properly accounted for. If a great wealth of information is available in the articles reporting on the selected cases, then further research work is absolutely required.

Except for those dedicated to solar cells for space missions, the studies are not driven by a specific application, and some of them cover a wide temperature range. Optimal design is likely to be less challenging if temperature and concentration factor ranges are restricted with respect to the targeted application. Also, in operation, the temperature of the solar cell results from the illumination, heat generation within the system, and heat exchanges with the environment. Hence, it seems reasonable to define first a set of specifications according to the desired functionalities. Almost always non-existent, specifications related to heat generation and exchanges are very different, depending on the application. For space missions, heat generation in the cells must be minimized, while heat exchanged with the environment must be maximized, to prevent an excessive temperature increase. On the contrary, in the case of terrestrial hybrid systems involving solar-to-thermal energy conversion devices, heat generation is essential so as to transfer this heat to the thermal part of the converter (fluid in motion, thermoelectric element, heat engine). Consequently, the design of the solar cells operating under thermal stress should consider these thermal-management criteria, meaning in particular that specific optical solutions will be needed for filtering out or absorbing photons with energy below the bandgap, while keeping maximum absorption of photons useful for the photovoltaic effect.

In each case, a great deal of research is needed to fill the gaps. With a prior accurate knowledge of the optical, electrical, and thermal properties at the operating temperature, the application of the usual design, fabrication, and characterization steps, new classes of solar cells withstanding temperatures from 100°C to 400°C—possibly even higher—could be developed in the near future. Aging under thermal-stress and life-cycle assessments would have to be carried out. Finally, it is worth mentioning the existence of solar cells operating at the opposite side of the temperature scale. These are PV devices for deep space missions working in low-intensity low-temperature (LILT) environments,[74] or even in terrestrial conditions in which the idea to intentionally cool cells down to the 111 K liquefaction temperature of liquified natural gas was proposed for boosting efficiency.[75] Similarly, a comprehensive set of research studies are required to develop solar cells specifically for low-temperature conditions.

## ACKNOWLEDGMENTS

This work was developed in the frame of the French program Investments for the Future managed by the National Agency for Research under contract ANR-10-LABX-22-01-SOLSTICE. C.L. is lecturer of the Serra Húnter programme. D.C. thanks the Institució Catalana de Recerca i Estudis Avançats (ICREA) for the ICREA Acadèmia, and the Ministerio de Ciencia e Innovación (project PID2019-111536RB-I00).

## AUTHOR CONTRIBUTIONS

D.C., R.V., and S.P. conceived the review analysis. R.V. researched most of the data, carried out most of the analysis, and wrote most of the article. S.P. researched the data, carried out the analysis, and wrote the sections dedicated to the contacts,

ARCs, TJs, and testing procedures. D.C., S.P., and R.V. contributed to the discussion of content. All of the authors edited the manuscript before submission.

## DECLARATION OF INTERESTS

The authors declare no competing interests.

## REFERENCES


1. Dupré, O., Vaillon, R., and Green, M.A. (2017). Thermal Behavior of Photovoltaic Devices. Physics and Engineering (Springer).
2. Scheiman, D.A., Landis, G.A., and Weizer, V.G. (1999). High-bandgap solar cells for near-Sun missions. In AIP Conference Proceedings, pp. 616–620.
3. Dakermanji, G., Jenkins, J., and Ercol, C. (2006). The messenger spacecraft solar array design and early mission performance. In 2006 IEEE 4th World Conference on Photovoltaic Energy Conference (IEEE), pp. 1919–1922.
4. Zimmermann, C.G., Nömayr, C., Kolb, M., and Caon, A. (2011). A solar cell design for the BepiColombo high intensity-high temperature mission. In 37th IEEE Photovolt. Spec. Conf (IEEE), pp. 3713–3718.
5. Loehberg, A., Gruenwald, C., Birkel, J., Brandl, A., Kuebler, N., Perrin, H., Andreev, T., Schuhmacher, U., and Taylor, S. (2017). The BepiColombo Mercury Planetary Orbiter (MPO) Solar Array Design, Major Developments and Qualification. E3S Web Conf. *16*, 04006.
6. Luque, A., and Hegedus, S. (2003). Handbook of Photovoltaic Science, A. Luque and S. Hegedus, eds. (John Wiley & Sons).
7. Merritt, D., Houlihan, S., Raffaelle, R.P., and Landis, G.A. (2005). Wide-bandgap space solar cells. In 31st IEEE Photovoltaic Specialists Conference (IEEE), pp. 552–555.
8. Branz, H.M., Regan, W., Gerst, K.J., Borak, J.B., and Santori, E.A. (2015). Hybrid solar converters for maximum exergy and inexpensive dispatchable electricity. Energy Environ. Sci. *8*, 3083–3091.
9. Bermel, P., Yazawa, K., Gray, J.L., Xu, X., and Shakouri, A. (2016). Hybrid strategies and technologies for full spectrum solar conversion. Energy Environ. Sci. *9*, 2776–2788.
10. Zondag, H.A. (2008). Flat-plate PV-Thermal collectors and systems: a review. Renew. Sustain. Energy Rev. *12*, 891–959.
11. Mellor, A., Alonso Alvarez, D., Guarracino, I., Ramos, A., Riverola Lacasta, A., Ferre Llin, L., Murrell, A.J., Paul, D.J., Chemisana, D., Markides, C.N., et al. (2018). Roadmap for the next-generation of hybrid photovoltaic-thermal solar energy collectors. Sol. Energy *174*, 386–398.
12. Huen, P., and Daoud, W.A. (2017). Advances in hybrid solar photovoltaic and thermoelectric generators. Renew. Sustain. Energy Rev. *72*, 1295–1302.
13. Narducci, D., Bermel, P., Lorenzi, B., Wang, N., and Yazawa, K. (2018). Hybrid and Fully Thermoelectric Solar Harvesting (Springer).
14. Shittu, S., Li, G., Akhlaghi, Y.G., Ma, X., Zhao, X., and Ayodele, E. (2019). Advancements in thermoelectric generators for enhanced hybrid photovoltaic system performance. Renew. Sustain. Energy Rev. *109*, 24–54.
15. Lorenzi, B., and Chen, G. (2018). Theoretical efficiency of hybrid solar thermoelectric-photovoltaic generators. J. Appl. Physiol. *124*, 024501.
16. Vossier, A., Zeitouny, J., Katz, E.A., Dollet, A., Flamant, G., and Gordon, J.M. (2018). Performance bounds and perspective for hybrid solar photovoltaic/thermal electricity-generation strategies. Sustain. Energy Fuels *2*, 2060–2067.
17. Luque, A., and Martí, A. (1999). Limiting efficiency of coupled thermal and photovoltaic converters. Sol. Energy Mater. Sol. Cells *58*, 147–165.
18. Dupré, O., Vaillon, R., and Green, M.A. (2015). Physics of the temperature coefficients of solar cells. Sol. Energy Mater. Sol. Cells *140*, 92–100.
19. Vaillon, R., Dupré, O., Cal, R.B., and Calaf, M. (2018). Pathways for mitigating thermal losses in solar photovoltaics. Sci. Rep. *8*, 13163.
20. Kurtz, S., Whitfield, K., Tamizhmani, G., Koehl, M., Miller, D., Joyce, J., Wohlgemuth, J., Bosco, N., Kempe, M., and Zgonena, T. (2011). Evaluation of high-temperature exposure of photovoltaic modules. Prog. Photovolt. Res. Appl. *19*, 954–965.
21. Guillemoles, J.F., Kirchartz, T., Cahen, D., and Rau, U. (2019). Guide for the perplexed to the Shockley–Queisser model for solar cells. Nat. Photonics *13*, 501–505.
22. Hirst, L.C., and Ekins-Daukes, N.J. (2011). Fundamental losses in solar cells. Prog. Photovolt. Res. Appl. *19*, 286–293.
23. Vaĭnshteĭn, I.A., Zatsepin, A.F., and Kortov, V.S. (1999). Applicability of the empirical varshni relation for the temperature dependence of the width of the band gap. Phys. Solid State *41*, 905–908.
24. Green, M.A. (1990). Intrinsic concentration, effective densities of states, and effective mass in silicon. J. Appl. Physiol. *67*, 2944–2954.
25. Galeckas, A., Grivickas, P., Grivickas, V., Bikbajevas, V., and Linnros, J. (2002). Temperature dependence of the absorption coefficient in 4H- and 6H-silicon carbide at 355 nm laser pumping wavelength. Phys. Status Solidi Appl. Res. *191*, 613–620.
26. Vurgaftman, I., Meyer, J.R., and Ram-Mohan, L.R. (2001). Band parameters for III-V compound semiconductors and their alloys. J. Appl. Physiol. *89*, 5815–5875.
27. Varshni, Y.P. (1967). Temperature dependence of the energy gap in semiconductors. Physica *34*, 149–154.
28. Zeitouny, J., Lalau, N., Gordon, J.M., Katz, E.A., Flamant, G., Dollet, A., and Vossier, A. (2018). Assessing high-temperature photovoltaic performance for solar hybrid power plants. Sol. Energy Mater. Sol. Cells *182*, 61–67.
29. Green, M.A. (2012). Limiting photovoltaic efficiency under new ASTM International G173-based reference spectra. Prog. Photovolt. Res. Appl. *20*, 954–959.
30. Nayak, P.K., Mahesh, S., Snaith, H.J., and Cahen, D. (2019). Photovoltaic solar cell technologies: analysing the state of the art. Nat. Rev. Mater. *4*, 269–285.
31. Dupré, O., Vaillon, R., and Green, M.A. (2016). A full thermal model for photovoltaic devices. Sol. Energy *140*, 73–82.
32. Braun, A., Katz, E.A., and Gordon, J.M. (2012). Basic aspects of the temperature coefficients of concentrator solar cell performance parameters. Prog. Photovolt. Res. Appl. *21*, 1087–1094.
33. Cuevas, A. (2014). The recombination parameter J0. Energy Procedia *55*, 53–62.
34. Piprek, J. (2003). Semiconductor Optoelectronic Devices: Introduction to Physics and Simulation (Academic Press).
35. Hassan, A., Savaria, Y., and Sawan, M. (2018). GaN integration technology, an ideal candidate for high-temperature applications: a review. IEEE Access *6*, 78790–78802.
36. Dupré, O., Vaillon, R., and Green, M.A. (2016). Experimental assessment of temperature coefficient theories for silicon solar cells. IEEE J. Photovoltaics *6*, https://doi.org/10.1109/JPHOTOV.2015.2489864.
37. Green, M.A. (1981). Solar cell fill factors: general graph and empirical expressions. Solid-State Electron. *24*, 788–789.
38. Friedman, D.J. (1996). Modelling of tandem cell temperature coefficients. In 25th IEEE Photovoltaic Specialists Conference (IEEE), pp. 89–92.
39. Raffaelle, R.P., Bailey, S.G., Neudeck, P., Okojie, R., Schnabel, C.M., Tabib-Azar, M., Scheiman, D., Jenkins, P., and Hubbard, S. (2000). Optical and electrical characterization of SiC devices. In 28th IEEE Photovoltaic Specialists Conference (IEEE), pp. 1257–1260.
40. Zhao, L., Detchprohm, T., and Wetzel, C. (2014). High 400 °C operation temperature blue spectrum concentration solar junction in GaInN/GaN. Appl. Phys. Lett. *105*, 243903.

41. Lien, D.-H., Hsiao, Y.-H., Yang, S.-G., Tsai, M.-L., Wei, T.-C., Lee, S.-C., and He, J.-H. (2015). Harsh photovoltaics using InGaN/GaN multiple quantum well schemes. Nano Energy *11*, 104–109.

42. Williams, J.J., McFavilen, H., Fischer, A.M., Ding, D., Young, S.R., Vadiee, E., Ponce, F.A., Arena, C., Honsberg, C.B., and Goodnick, S.M. (2016). Development of a high-band gap high temperature III-nitride solar cell for integration with concentrated solar power technology. In 43rd IEEE Photovoltaic Specialists Conference (IEEE), pp. 0193–0195.

43. Williams, J.J., Goodnick, S.M., McFavilen, H., Fischer, A.M., Ding, D., Young, S., Vadiee, E., Ponce, F.A., Arena, C., and Honsberg, C.B. (2017). Refractory Inx Ga1−x N solar cells for high-temperature applications. IEEE J. Photovoltaics *7*, 1646–1652.

44. Huang, X., Fu, H., Chen, H., Lu, Z., Baranowski, I., Montes, J., Yang, T.-H.T.H., Gunning, B.P.P., Koleske, D., and Zhao, Y. (2017). Reliability analysis of InGaN/GaN multi-quantum-well solar cells under thermal stress. Appl. Phys. Lett. *111*, 233511.

45. Zhao, Y., Huang, X., Fu, H., Chen, H., Lu, Z., Montes, J., and Baranowski, I. (2017). InGaN-based solar cells for space applications. In IEEE 60th International Midwest Symposium on Circuits and Systems (IEEE), pp. 954–957.

46. Perl, E.E., Simon, J., Geisz, J.F., Lee, M.L., Friedman, D.J., and Steiner, M.A. (2016). Measurements and modeling of III-V solar cells at high temperatures up to 400°C. IEEE J. Photovoltaics *6*, 1345–1352.

47. Perl, E.E., Simon, J., Geisz, J.F., Olavarria, W., Young, M., Duda, A., Friedman, D.J., and Steiner, M.A. (2016). Development of high-bandgap AlGaInP solar cells grown by organometallic vapor-phase epitaxy. IEEE J. Photovoltaics *6*, 770–776.

48. Perl, E.E., Kuciauskas, D., Simon, J., Friedman, D.J., and Steiner, M.A. (2017). Identification of the limiting factors for high-temperature GaAs, GaInP, and AlGaInP solar cells from device and carrier lifetime analysis. J. Appl. Physiol. *122*, 233102.

49. Philipps, S.P., Hoheisel, R., Gandy, T., Stetter, D., Hermle, M., Dimroth, F., and Bett, A.W. (2011). An experimental and theoretical study on the temperature dependence of GaAs solar cells. In 37th IEEE Photovoltaic Specialists Conference (IEEE), pp. 1610–1614.

50. Bett, A.W., Dimroth, F., Hermle, M., Hoheisel, R., Stetter, D., and Philipps, S.P. (2008). Characterization and numerical modeling of the temperature-dependent behavior of GaAs solar cells. In 23rd Eur. Photovolt. Sol. Energy Conf. Exhib., pp. 114–117.

51. Maros, A., Gangam, S., Fang, Y., Smith, J., Vasileska, D., Goodnick, S., Bertoni, M.I., and Honsberg, C.B. (2015). High temperature characterization of GaAs single junction solar cells. In 42nd IEEE Photovoltaic Specialists Conference (IEEE), pp. 1–5.

52. Sun, Y., Faucher, J., Jung, D., Vaisman, M., McPheeters, C., Sharps, P., Perl, E., Simon, J., Steiner, M., Friedman, D., et al. (2016). Thermal stability of GaAs solar cells for high temperature applications. In 43rd IEEE Photovoltaic Specialists Conference (IEEE), pp. 2385–2388.

53. Vadiee, E., Fang, Y., Zhang, C., Fischer, A.M., Williams, J.J., Renteria, E.J., Balakrishnan, G., and Honsberg, C.B. (2018). Temperature dependence of GaSb and AlGaSb solar cells. Curr. Appl. Phys. *18*, 752–761.

54. Steiner, M.A., Perl, E.E., Simon, J., Friedman, D.J., Jain, N., Sharps, P., McPheeters, C., and Lee, M.L. (2017). AlGaInP/GaAs tandem solar cells for power conversion at 400°C and high concentration. In AIP Conf. Proc, *1881*.

55. Perl, E.E., Simon, J., Friedman, D.J., Jain, N., Sharps, P., McPheeters, C., Sun, Y., Lee, M.L., and Steiner, M.A. (2018). (Al)GaInP/GaAs Tandem Solar Cells for Power Conversion at Elevated Temperature and High Concentration. IEEE J. Photovoltaics *8*, 640–645.

56. Steiner, M.A., Perl, E.E., Simon, J., Friedman, D.J., Jain, N., Sharps, P., McPheeters, C., and Lee, M.L. (2017). AlGaInP/GaAs tandem solar cells for power conversion at 400°C and 1000X concentration. In 44th IEEE Photovoltaic Specialists Conference (IEEE), pp. 42–45.

57. Nishioka, K., Takamoto, T., Agui, T., Kaneiwa, M., Uraoka, Y., and Fuyuki, T. (2005). Evaluation of temperature characteristics of high-efficiency InGaP/InGaAs/Ge triple-junction solar cells under concentration. Sol. Energy Mater. Sol. Cells *85*, 429–436.

58. Steiner, M.A., Geisz, J.F., Friedman, D.J., Olavarria, W.J., Duda, A., and Moriarty, T.E. (2011). Temperature-dependent measurements of an inverted metamorphic multijunction (IMM) solar cell. In 37th IEEE Photovoltaic Specialists Conference (IEEE).

59. Geisz, J.F., Kurtz, S., Wanlass, M.W., Ward, J.S., Duda, A., Friedman, D.J., Olson, J.M., McMahon, W.E., Moriarty, T.E., and Kiehl, J.T. (2007). High-efficiency GaInP GaAs InGaAs triple-junction solar cells grown inverted with a metamorphic bottom junction. Appl. Phys. Lett. *91*, 1–4.

60. Geisz, J.F., Friedman, D.J., Ward, J.S., Duda, A., Olavarria, W.J., Moriarty, T.E., Kiehl, J.T., Romero, M.J., Norman, A.G., and Jones, K.M. (2008). 40.8% efficient inverted triple-junction solar cell with two independently metamorphic junctions. Appl. Phys. Lett. *93*, 40–42.

61. Brandt, C., Baur, C., Caon, A., Müller-Buschbaum, P., Zimmermann, C., and Andreev, T. (2013). The influence of high temperatures on radiation damage of GaInP2/GaAs/Ge triple junction cells. IEEE J. Photovoltaics *3*, 904–908.

62. Brandt, C., Hulsheger, T., Baur, C., Caon, A., and Andreev, T. (2011). The influence of high light inclination angles on the performance of GaInP2/GaAs/Ge triple junction solar cells. In 37th IEEE Photovoltaic Specialists Conference (IEEE), pp. 1572–1578.

63. Elarde, V.C., Cardwell, D., Hillier, G., Wibowo, A., Hoheisel, R., Gonzalez, M., Lumb, M., Tomasulo, S., Kotulak, N., Scheiman, D., et al. (2016). High-temperature (450°C) operation of InGaP solar cell under N2 ambient using refractory metal contacts. In 43rd IEEE Photovoltaic Specialists Conference (IEEE), pp. 2337–2340.

64. Landis, G.A., Jenkins, P., Scheimant, D., and Ryne, R. (2004). Extended temperature solar cell technology development. In 2nd International Energy Conversion Engineering Conference, pp. 1–7.

65. Colter, P., Hagar, B., and Bedair, S. (2018). Tunnel junctions for III-V multijunction solar cells review. Crystals (Basel) *8*, 445.

66. Braun, A., Hirsch, B., Katz, E.A., Gordon, J.M., Guter, W., and Bett, A.W. (2009). Localized irradiation effects on tunnel diode transitions in multi-junction concentrator solar cells. Sol. Energy Mater. Sol. Cells *93*, 1692–1695.

67. Vossier, A., Chemisana, D., Flamant, G., and Dollet, A. (2012). Very high fluxes for concentrating photovoltaics: Considerations from simple experiments and modeling. Renew. Energy *38*, 31–39.

68. Schroder, D.K. (2015). Semiconductor Material and Device Characteziation, Third Edition (Wiley-IEEE).

69. Galiana, B., Algora, C., Rey-Stolle, I., and García Vara, I. (2005). A 3-D model for concentrator solar cells based on distributed circuit units. IEEE Trans. Electron Dev. *52*, 2552–2558.

70. Steiner, M.A., Siefer, G., and Bett, A.W. (2014). An investigation of solar cell interconnection schemes within CPV modules using a validates temperature-dependent SPICE network model. Prog. Photovolt. Res. Appl. *22*, 505–514.

71. Burdick, J., and Glatfelter, T. (1986). Spectral response and I-V measurements of tandem amorphous-silicon alloy solar cells. Sol. Cells *18*, 301–314.

72. Meusel, M., Baur, C., Létay, G., Bett, A.W., Warta, W., and Fernandez, E. (2003). Spectral response measurements of monolithic GaInP/Ga(In)As/Ge triple-junction solar cells: Measurement artifacts and their explanation. Prog. Photovolt. Res. Appl. *11*, 499–514.

73. Grandidier, J., Kirk, A.P., Jahelka, P., Stevens, M.A., Gogna, P.K., Crisp, D., Osowski, M.L., Vandervelde, T.E., Atwater, H.A., and Cutts, J.A. (2020). Photovoltaic operation in the lower atmosphere and at the surface of Venus. Prog. Photovolt. Res. Appl. *28*, 545–553.

74. Hoheisel, R., Bett, A.W., Warner, J.H., Walters, R.J., and Jenkins, P.P. (2018). Low Temperature Low Intensity Effects in III-V Photovoltaic Devices for Deep Space Missions. In 2018 IEEE 7th World Conference on Photovoltaic Energy Conversion, WCPEC 2018 - A Joint Conference of 45th IEEE PVSC, 28th PVSEC and 34th EU PVSEC (Institute of Electrical and Electronics Engineers Inc.), pp. 3763–3767.

75. Gordon, J.M., Moses, G., and Katz, E.A. (2021). Boosting silicon photovoltaic efficiency from regasification of liquefied natural gas. Energy *214*, 118907.

76. Sze, S.M., and Ng, K.K. (2007). Physics of Semiconductor Devices, Third Edition (Wiley).